A Li2CO3-Free Li-O2/CO2 Battery with Peroxide Discharge Product

Journal:	*Energy & Environmental Science*
Manuscript ID	EE-COM-11-2017-003341.R2
Article Type:	Communication
Date Submitted by the Author:	28-Feb-2018
Complete List of Authors:	QIAO, Yu; AIST, Yi, Jin; AIST Guo, Shaohua ; NJU, College of Engineering and Applied Science Sun, Yang; AIST Wu, Shichao; AIST, Liu, Xizheng; Tianjin University of Technology, Institute for New Energy Materials and Low-Carbon Technologies; Yang, Sixie; Nanjing University He, Ping; Nanjing University, College of Engineering and Applied Sciences; National Institute of Advanced IndustrialScience and Technology , Energy Technology Research Institute Zhou, HaoShen; AIST,

COMMUNICATION Journal Name

A Li_2CO_3-Free Li-O_2/CO_2 Battery with Peroxide Discharge Product

Yu Qiao,[a,c] Jin Yi,[a] Shaohua Guo,[b] Yang Sun,[a] Shichao Wu,[a] Xizheng Liu,[d] Sixie Yang,[b] Ping He,[b] and Haoshen Zhou[a,b,c]*

Received 00th January 20xx,
Accepted 00th January 20xx

DOI: 10.1039/x0xx00000x

www.rsc.org/

Owing to its exceptionally high energy potentiality based on Lithium-oxygen chemistry, Lithium-air battery has been boosted as an appealing alternative to current state-of-art Lithium-ion batteries. However, due to the presence of non-O_2 components in ambient air, the practical performance of Li-air battery is limited to only few cycles with low energy efficiency. Particularly, once CO_2 being incorporated in battery system, Li_2CO_3 would inevitably formed during discharging, which results serious climbing of charge potential and relevant decomposition of cell components. Herein, with appropriate introduction of electrolyte into aggregated contact-ion-pair (CIP) structure, we demonstrate a Li-O_2/CO_2 battery cycles via stabilized peroxodicarbonate ($C_2O_6^{2-}$) formation in electrolyte rather than Li_2CO_3, and operates with a very low charge potential (3.5 V). We anticipate that this discovery will provide a rational design strategy for modifying the reaction pathway of Li-O_2/CO_2 battery, and accelerate the step of evolution from Li-O_2 to Li-air batteries.

The remarkably increasing demand for high-energy rechargeable batteries has heightened considerable interests in aprotic Li-air batteries, which can deliver extremely high theoretical gravimetric energy (calculated form reaction of Li and O_2) compared to conventional Li-ion batteries.[1, 2] In fact, most of Li-air batteries have demonstrated cell operations in pure O_2 atmosphere, because the presence of other constituents in ambient air (H_2O, CO_2, etc.) would inevitably alter reaction pathway and lead to the formation of parasitic products such as LiOH and Li_2CO_3, resulting poor cyclability and high polarization.[3-5] However, in order to remove these complications, the introduction of the additional gas purification components leads to substantial increase in the weight and capital cost of battery system, which ineluctably counteract its most sparkling advantage, high energy density.[6] In this case, the development of practical Li-ambient air battery deeply sinks into dilemma.

Recently, the role of water in Li-O_2 system has been revealed as a helpful proton-donor.[7, 8] Moreover, as another influential air component, CO_2 is of particular interest due to its high solubility in organic electrolyte solvents (~50 times more soluble than O_2) and reactivity with superoxide anion (O_2^-), the key intermediate and the crime culprit of nucleophilic attack in Li-O_2 battery.[3, 9-12] Therefore, involving CO_2 within Li-O_2 cell would be a center point of penetration for the evolution from Li-O_2 to Li-air system. Recently, by suppressing the superoxide-related parasitic reactions, a rechargeable Li-O_2/CO_2 battery based on Li_2CO_3 has been introduced with a boosted discharge capacity compared with typical Li-O_2 battery.[13, 14] However, the charge voltage was locked above the thermodynamic voltage for the decomposition of Li_2CO_3 (3.82 V vs. Li/Li^+),[3, 15] which lead to low round-trip efficiency (nearly 67 %) and decomposition of other cell components, resulting in rapid cell degradation after several cycles.[14, 16] Besides, the high overpotential appears in Li-O_2 cell can also, to some extent, be ascribed to the parasitic production of Li_2CO_3.[17, 18] In this case, the high decomposition potential of Li_2CO_3 become the insurmountable barrier limits the practical application of Li-O_2/CO_2 and Li-air batteries. Although, early works on CO_2-incorporated aprotic oxygen reduction process proposed the formation of superoxocarbonate (CO_4^-) and/or peroxocarbonate ($C_2O_6^{2-}$) as probable intermediates, which may deliver lower decomposition potential than carbonate,[3, 9, 10] these metastable intermediates would rapidly suffer from further reduction/dissociation into Li_2CO_3.

Thus, effectively interdicting the direct interaction between Li-ion and these metastable intermediate anion would be a feasible solution to stabilize these intermediates and introduce them into the reversible cycle in Li-O_2/CO_2 system. Recent studies reveals that both the solvation state of Li-ion and the structure of entire electrolyte system can be essentially controlled by adjusting the concentration of salt with specific anion, especially in electrolyte with high dielectric solvent such as dimethyl sulfoxide (DMSO).[19-22] In this work, enlightened by the unique features of super-concentrated electrolytes,[23] we further introduce a aggregated electrolyte system composed of DMSO-sheathed contact-ion-pair (CIP). Different from diluted electrolytes, the polymeric fluid network composed in our specific-introduced electrolyte would efficiently stabilize peroxodicarbonate species by effectively restrain its incorporation with Li^+. Consequently, we demonstrate a

[a] Energy Technology Research Institute, National Institute of Advanced Industrial Science and Technology (AIST), 1-1-1, Umezono, Tsukuba 305-8568, Japan. hs.zhou@aist.go.jp (H. Z.)
[b] National Laboratory of Solid State Microstructures & Department of Energy Science and Engineering, Nanjing University, Nanjing 210093, P. R. China. hszhou@nju.edu.cn (H. Z.)
[c] Graduate School of System and Information Engineering, University of Tsukuba, 1-1-1, Tennoudai, Tsukuba 305-8573, Japan.
[d] Tianjin Key Laboratory of Advanced Functional Porous Materials, Institute for New Energy Materials and Low-Carbon Technologies, School of Material Science and Engineering, Tianjin University of Technology, Tianjin 300384, P. R. China.
Electronic Supplementary Information (ESI) available: [details of any supplementary information available should be included here]. See DOI: 10.1039/x0xx00000x

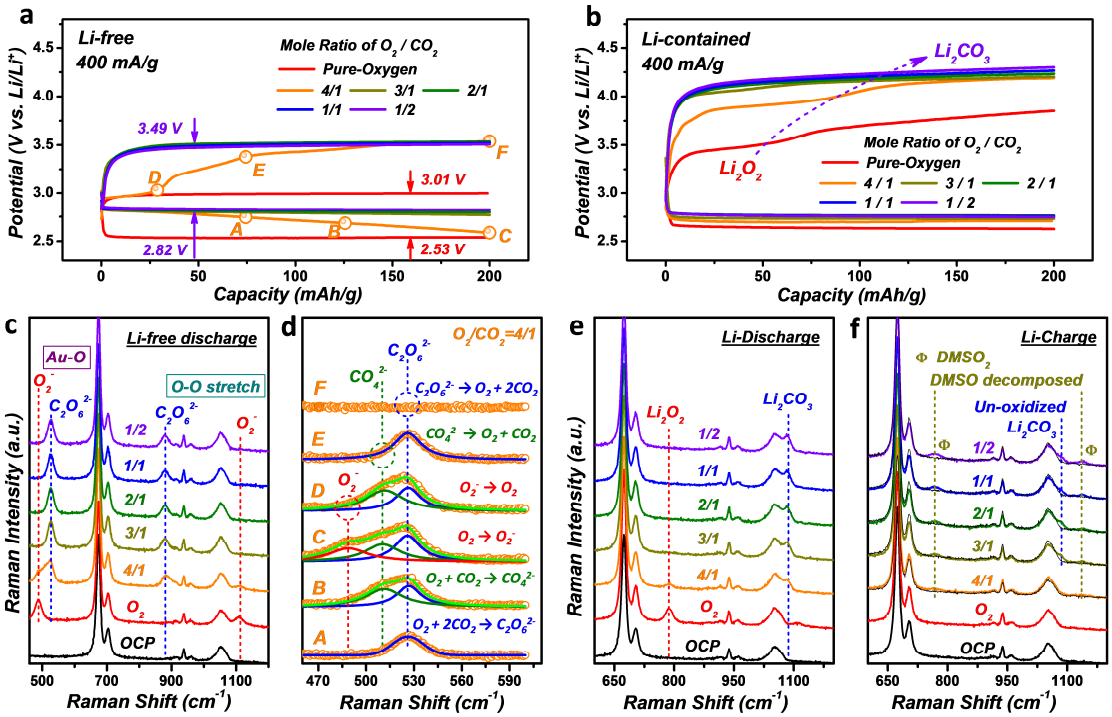

Figure 1. Influence of CO_2 towards aprotic oxygen reduction. Galvanostatic discharge/charge profiles of cells with various volume ratio of O_2/CO_2 mixed gas at 400 mA/g current density in (a) Li-free $TBAClO_4$/DMSO (Li-free) and (b) $LiClO_4$/DMSO (Li-contained) electrolyte. In-situ Raman spectra recorded at corresponding discharge/charge states: (c) End of discharge states recorded from Li-free cells with various O_2/CO_2 ratios; (d) Specific points recorded during cycling in Li-free cell with specific O_2/CO_2 ratio (4/1 volume ratio), and the spectra are fitted by Gaussian-Lorentzian distribution functions with corresponding reaction steps listed inset; Spectra collected at the end of each discharge (e) and corresponding charge (f) states in Li-contained cells with various O_2/CO_2 ratios. The colors and electrochemical behaviors of in-situ Raman spectra are consistent with each of their galvanostatic curves shown above.

Li-O_2/CO_2 battery with an ultralow charge potential (3.5 V vs. Li/Li^+) and considerable cycle life. More importantly, free of typical Li_2CO_3, the newly-proposed battery cycles via pure peroxodicarbonate formation, which not only remedies the inherent defects in CO_2-incorporated Li-O_2 electrochemistry but also paves the way for more practical Li-air battery system.

Firstly, we want to clarify the influence of CO_2 towards aprotic oxygen reduction process. As a remarkably powerful operando characterization method, in-situ Raman spectroscopy with surface enhanced nanoporous gold (NPG, Figure S1) substrate is preferentially employed to investigate the reaction mechanism (Figure S2).[24, 25] Excluding the influence of Li-ion, related discharge products have been initially investigated in gas saturated 0.5 M tetrabutylammonium perchlorate ($TBAClO_4$)-DMSO electrolyte. Without CO_2, pure oxygen reduction/oxidation operate upon flat discharge/charge plateaus (2.53/3.01 V, Figure 1a), which ascribe to the conventional O_2/O_2^- redox couple.[26] Exemplified by Raman spectra obtained at corresponding discharge state (red trace, Figure 1c), regardless of the strong peaks from DMSO (Figure S3), the newly-produced peaks can be assigned to Au-O (488 cm^{-1}) and O-O (1108 cm^{-1}) stretches in adsorbed superoxide anion.[27] After trace CO_2 being introduced (orange trace, 4/1 volume ratio of O_2/CO_2, Figure 1c), the discharge potential rapidly climbs up and the corresponding charge curve also distorts into several stages. Segmented analysis (Figure 1d) reveals that peroxodicarbonate ($C_2O_6^{2-}$) formed during initial discharging (Figure S4 and S5), which has been further verified by the chemically synthesized species (Figure S6). The related assignment and extended discussion on the reaction pathway and peroxo configuration have been exhibited in Figure S7 and S8. With the consumption of CO_2, peroxomonocarbonate (CO_4^{2-}) is subsequently validated by the observation of another Au-O adsorption peak appears at lower wavenumber (green peak, point-B, Figure 1d). Continuously, the discharge process returns to the typical oxygen reduction with the production of O_2^- (red peak, point-C, Figure 1d). With the sequential disappearing of corresponding Raman stretches shown in Figure 1d, the subsequent charge process conducts in the order of thermodynamic equilibrium potential of specific reactions:[3]

Point C to D (red peak): $O_2^- \rightarrow O_2 + e^-$ (E_1 = 2.64 V vs. Li/Li^+)
Point D to E (green peak): $CO_4^{2-} \rightarrow O_2 + CO_2 + 2e^-$ (E_2 = 2.89 V)
Point E to F (blue peak): $C_2O_6^{2-} \rightarrow O_2 + 2CO_2 + 2e^-$ (E_3 = 3.27 V)

Continuously increasing the ratio of CO_2, the discharge processes are fixed within pure $C_2O_6^{2-}$ production, and the charging processes are also stabilized at peroxodicarbonate-related 3.49 V plateau. The variation of surface electrochemistry can be ascribed to the relationship between gas diffusion coefficient and related gas consumption rate (current-dependent) within the double electrode layer. The discussion of related dynamic issue has been extended in Figure S8.

However, once Li-ion being introduced, the charge potential plateau quickly rises up to 4.2 V (Figure 1b), and the corresponding Raman results (Figure 1e) demonstrate that

related discharge products are converted from Li_2O_2 to Li_2CO_3 in CO_2 incorporated condition. More seriously, not only the Li_2CO_3 cannot be fully decomposed after charging, but the high polarized voltage inevitably leads to the formation of $DMSO_2$, a parasitic product of DMSO oxidization (Figure 1f).[28] Herein, the highly polarization overpotential and the related rigid Li_2CO_3 decomposition process also present well coincide with our previous results.[29, 30] Consequently, the parasitic reaction and irreversibility directly result in the degradation of cell after merely several cycles (Figure S9). The failure of cell would only become worse on practical carbon-based cathodes due to the decomposition of carbon on high potential.[16, 18] In summary, the high decomposition potential of Li_2CO_3, the final stable discharge product, directly leads to the instability of the typical Li-O_2/CO_2 battery system. Although the peroxodicarbonate, a metastable intermediate, can stably exist in Li-free condition and achieve lower charge potential,[9] its cannot be effectively utilized due to the diffusion of Li-ion from metal Li anode during a long term running (Figure S10). Enlighten by the redox mediator strategy in Li-O_2 battery system,[31, 32] how to essentially restrain the rigid Li_2CO_3-related reaction pathway, the intrinsic defect for Li-O_2/CO_2 battery, and efficiently stabilize the soluble peroxodicarbonate product in Li-contained cell become one of the most feasible modification routes.

In dilute electrolyte (Figure 2a), the interaction between $[Li(DMSO)_n]^+$ solvation sphere cation and $TFSI^-$ anion is relatively weak, providing the opportunity for the incorporation between Li^+ cation and $C_2O_6^{2-}$ anion. This directly leads to the further reduction and dissociate breakage of the peroxide O-O bridge, resulting in the formation of Li_2CO_3.[3] Thus, interdicting the electric interaction between Li^+ and $C_2O_6^{2-}$ presents as the most essential solution pathway. Neutralizing the charge on Li^+ cation by strengthening its interaction with other anion would be a feasible route. Typically, the solvation number of Li^+ in DMSO solution has been confirmed as 4.0, which indicates a $[Li(DMSO)_4]^+$ mono-dentate ligand.[21] Herein, we further increase the salt concentration and replace one of the DMSO molecule among the solvation sheath into a larger anion, for example bis(trifluoromethylsulfonyl)amide ($TFSI^-$). Based on the concentration-dependent Raman spectra recorded from various LiTFSI-DMSO electrolytes (Figure 2b and S11), the C-S stretching modes in free DMSO (red peaks, 669/699 cm^{-1}) gradually decrease with the increasing salt concentrations, while the corresponding modes in solvated DMSO (green peaks, 680/713 cm^{-1}) become dominate. Note that, only the solvated DMSO can be observed in specific super-concentrated electrolyte with 1:3 mole ratio (LiTFSI:DMSO) which indicates that the complex with $[Li(DMSO)_3]^+$-$[TFSI^-]$ aggregated structure has been achieved. More importantly, based on deeper analysis towards S-N stretching mode in $TFSI^-$, the ion

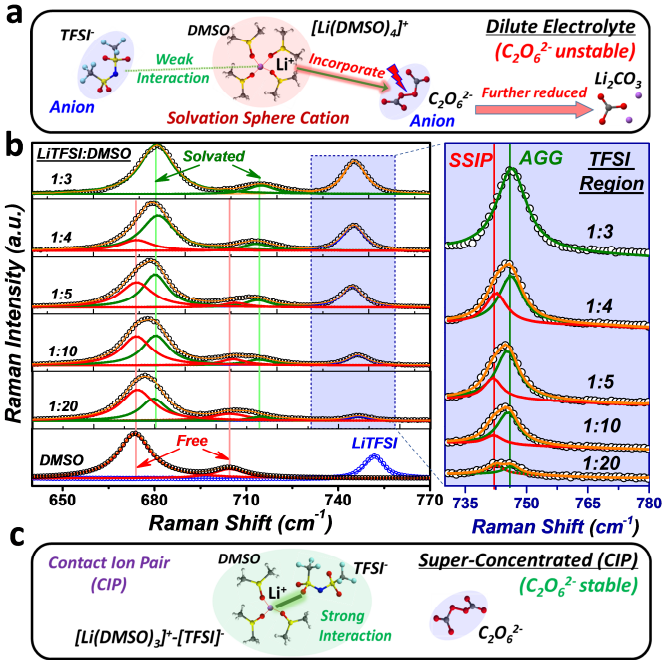

Figure 2. Design of electrolyte structure. (a) Schematic illustrations of electrolyte structure in dilute LiTFSI/DMSO-based Li-O_2/CO_2 cell, and relevant discharged components. As an intermediate, peroxodicarbonate ($C_2O_6^{2-}$) coordinates with solvated Li-ion and dissociates into Li_2CO_3 as the typical final product. (b) Raman spectra of LiTFSI/DMSO solutions with various mole ratios. Spectra are fitted by Gaussian-Lorentzian distribution functions, and the SNS stretch region in $TFSI^-$ (blue outlined) is magnified for clarity. In LiTFSI/DMSO electrolyte with 1:3 mole ratio, neither free DMSO molecule nor Solvent-Separated-Ion-Pair (SSIP) can be observed. Instead, sheathed by DMSO molecules, Li^+ and $TFSI^-$ is completely aggregated (AGG) within a Contact-Ion-Pair (CIP) fluid network. (c) Schematic illustration of the newly-introduced super-concentrated fluid network electrolyte composed of $[Li(DMSO)_3]^+$-$[TFSI^-]$. The electric interaction between Li^+ cation and $C_2O_6^{2-}$ anion could be effectively interdicted due to the electroneutrality of CIP-composed electrolyte system. As a result, the further reduction from $C_2O_6^{2-}$ to CO_3^{2-} could also be restrained.

association mode in super-concentrated electrolyte (1:3 mole ratio) entirely evolves from "solvent separated ion which indicates that the complex with $[Li(DMSO)_3]^+$-$[TFSI^-]$ aggregated structure has been achieved. More importantly, based on deeper analysis towards S-N stretching mode in $TFSI^-$, the ion association mode in super-concentrated electrolyte (1:3 mole ratio) entirely evolves from "solvent separated ion pair (SSIP)" into "contact ion pair (CIP)".[21, 33] As a result, without being sheathed into the solvated cation sphere in SSIP, Li^+ directly contacts with $TFSI^-$ and peripherically solvated by DMSO in CIP (Figure S12). Moreover, choosing suitable anion is also important, since the relative hard base (ClO_4^-, etc.) cannot fit well with softened huge $[Li(DMSO)_3]^+$ (Figure S13).[26] Consequently, being aggregated into polymeric fluid network (Figure 2c), Li^+ can be further trapped within the newly-introduced electrolyte network composed of CIPs, and the related interaction between Li^+ cation and peroxodicarbonate anion could be restrained.Besides, without the free DMSO molecules exist in typical diluted electrolyte system, other unique features have been revealed in concentrated electrolytes, such as high stability towards attack from nucleophilic superoxide radical, reductive Li metal and electrochemical oxidization (Figure S14 and S15).[20, 21]

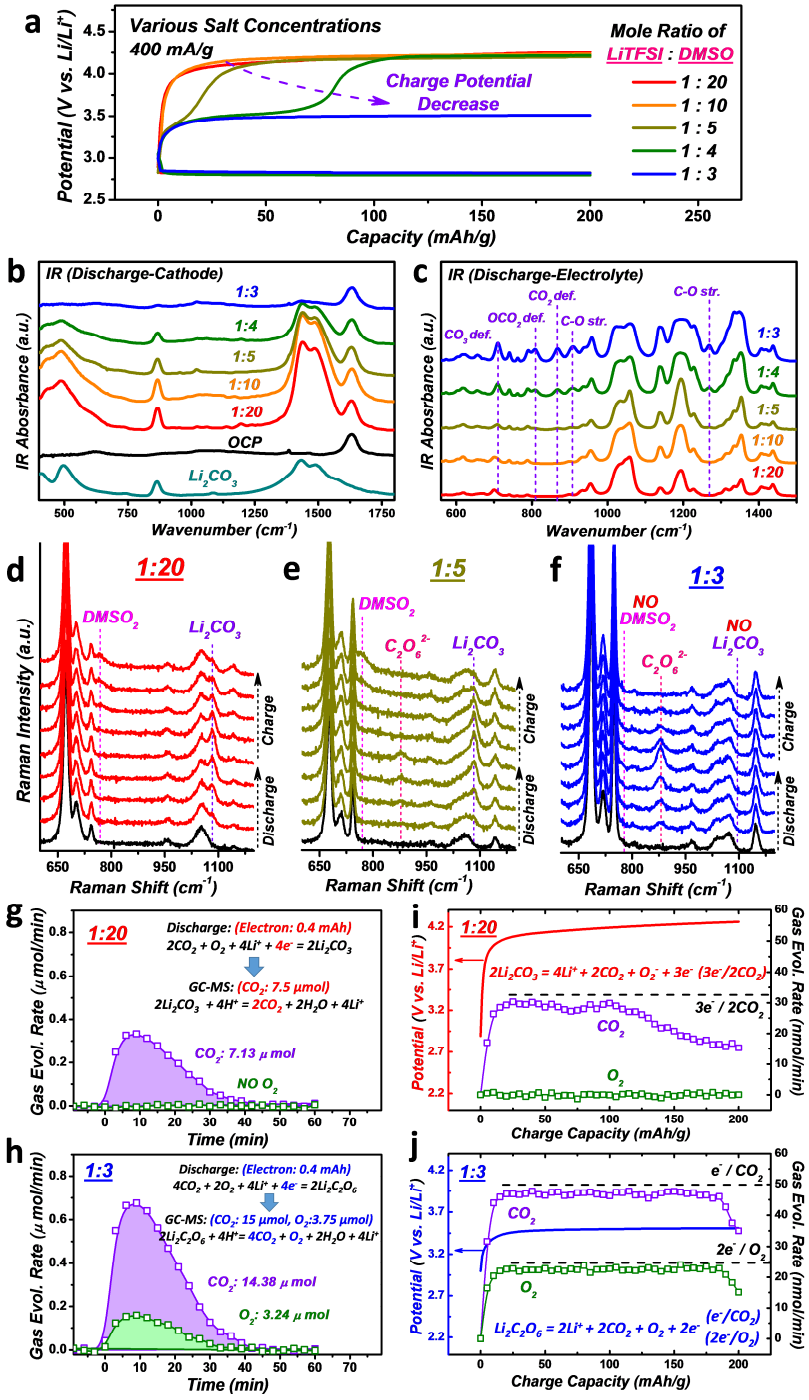

Figure 3. Electrochemistry and spectroscopy characterizations. (a) Voltage profiles of Li-O_2/CO_2 (1:1, volume ratio) cells operate in LiTFSI/DMSO electrolyte with different mole ratios (current density: 400 mA/g). b-c, IR spectra collected from the discharged cell components: (b) cathodes and (c) electrolytes. d-f, In-situ Raman spectra recorded during the 1st cycle from cells with various LiTFSI:DMSO mole ratios: (d) 1:20; (e) 1:5; (f) 1:3. g-h, Carbonate and peroxodicarbonate quantifications conducted on discharge cells (fixed 0.4 mAh capacity) with different LiTFSI:DMSO mole ratios: (g) 1:20 and (h) 1:3. CO_2 and O_2 evolution rates are collected after acid treatment, and the integrated amounts of gas (CO_2 and/or O_2) are compared with the corresponding theoretical amounts. The related reaction steps and quantitative comparison are inset for clarity. i-j, DEMS results of gas evolution rates for CO_2 and O_2 during charging in cells with different LiTFSI:DMSO mole ratios: (i) 1:20 and (j) 1:3. The electron number (versus CO_2 and O_2 gas molecule) marked by dash lines are corresponded to the specific reaction pathway listed inset.

Turning back to Li-O_2/CO_2 cell (Figure 3a), by employing highly-concentrated LiTFSI-DMSO electrolyte (1:5 and 1:4 mole ratios), charge plateaus gradually divide into two stages, with a lower peroxodicarbonate-related plateau (3.5 V) appears during initial (Figure 1a), which coincide with the pair of oxidization peaks observed during corresponding cathodic linear sweeping processes (Figure S16). In particular, the charging plateau keeps at 3.5 V in the electrolyte composed of CIPs (blue trace, 1:3 mole ratio). The relevant transition from carbonate to peroxodicarbonate has been corroborated by IR

results, in which the signal of deposited Li_2CO_3 (Figure 3b) gradually drops to invisible while the increasing of related adsorption peaks in dissolved peroxodicarbonate become dominated (Figure 3c and S17). Thorough charge plateau assignments are revealed by in-situ Raman investigations (Figure 3d-3f, S18). In dilute electrolyte (1:20, Figure 3d), the incompletely decomposition of Li_2CO_3 and parasitic oxidation of DMSO (form $DMSO_2$) are clearly revealed. Subsequently, trace signal of peroxodicarbonate appears in concentrated electrolyte during discharge (1:5, Figure 3e), however, production of Li_2CO_3 still exist and related high decomposition potential ineluctably leads to the formation of $DMSO_2$. Nevertheless, essential change occurs in CIP-composed electrolyte system (1:3, Figure 3f), in which the Li-O_2/CO_2 cell operates via pure peroxodicarbonate formation/decomposition.

More quantitative analysis towards discharge products are conducted based on carbonate/peroxo-species quantification by respectively monitoring CO_2/O_2 gas evolution rate after acid treatment.[34] Discharged product in conventional dilute system has been confirmed as pure Li_2CO_3 species without any O_2 releasement (Figure 3g). In stark contrast, O_2 evolution further confirms the formation of peroxo-species in super-concentrated electrolyte condition (Figure 3h). Moreover, compared with the theoretical value calculated based on fixed discharge capacity (0.4 mAh), the specific constituent contents of released O_2/CO_2 mixture present well coincide with the pure production of peroxodicarbonate ($C_2O_6^{2-}$), which is also consistent with the related titration results (Figure S19). Finally, differential electrochemical mass spectroscopy (DEMS) is employed to investigate the reaction reversibility by monitoring gas evolution rate.[34] In dilute electrolyte condition (Figure 3i), the rechargeable but irreversible nature of Li-O_2/CO_2 cell has been revealed due to the incomplete decomposition of Li_2CO_3 during charging, especially during the last period. As comparison, during the flat 3.5 V charging plateau conducted in super-concentrated electrolyte (Figure 3j), the obtained specific charge-to-mass ratios ($2e^-/O_2$ and e^-/CO_2) well follows the reaction pathway, which defined as: $C_2O_6^{2-} \rightarrow O_2 + 2CO_2 + 2e^-$. The details of DEMS characterization and corresponding overcharging investigation have been revealed in Figure S20 and S21, in which only trace amount of irreversible gas behavior (around 1.1%) can be observed. Combined with corresponding segmented titration results (Figure S22 and S23), within the margin of error, the peroxodicarbonate-based reversible electrochemical process has been successfully achieved in Li-O_2/CO_2 cell with CIP-composed electrolyte. Additionally, benefit from the specific solution-based charging process, the low charging potential can be well maintained, which is very similar as the one observed in the redox mediator involved Li-O_2 battery system (Figure S24). Moreover, the $C_2O_6^{2-}$-related electrochemical behavior can also be observed within the Li-O_2/CO_2 cell purged with varying gas ratios (Figure S25). More important, the peroxodicarbonate-related pathway can also be realized on a more practical cathode composed by porous carbon material (Figure S26 and S27), indicating the potential for the extension of the newly-proposed mechanism to more practical applications.

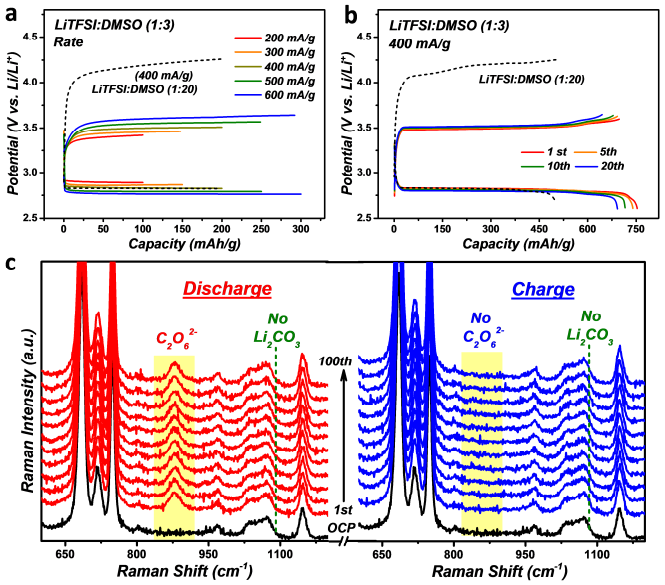

Figure 4. Electrochemical performance of Li-O_2/CO_2 batteries. a-b, Galvanostatic voltage profiles of Li-O_2/CO_2 (1:1, volume ratio) cells with specific LiTFSI/DMSO (1:3, mole ratio) electrolyte. (a) Initial cycle at current densities from 200 to 600 mA/g. (b) Full discharge-charge profiles over 20 cycles controlled by potential limits from 2.6 to 3.65 V at 400 mA/g. (c) In-situ Raman spectra collected at the end of each discharge (red) and charge (blue) states among typical cycles during cycling with a fixed capacity of 200 mAh/g (at 400 mA/g current density). The corresponding voltage profiles are shown in Figure S29.

For more practical utility, electrochemical performance of the Li-O_2/CO_2 battery with super-concentrated electrolyte has been revealed in Figure 4. With the current density raising from 200 to 600 mA/g (Figure 4a), the polarization degree do not drastically increase, and the charge plateau still keeps below 3.6 V at 600 mA/g (blue trace), which is far more below the voltage observed in typical Li-O_2/CO_2 battery operates with dilute electrolyte (black dash trace). Besides, the full discharge capacity has been extended to 753 mAh/g (2.6 V cutoff voltage), and most of the initial capacity (92%) is retained after 20 full cycles in super-concentrated electrolyte (Figure 4b and S28). More importantly, compared with the typical energy efficiency of Li-O_2/CO_2 cell performed in dilute electrolyte, the corresponding value has been significant promoted in our specific-designed battery system.[13, 14, 35] Furthermore, cycling with a cut-off capacity of 200 mAh/g (Figure S29), the corresponding cell exhibits a stable discharge/charge windows at 2.8/3.5 V over 100 cycles. Different from typical Li-O_2/CO_2 cells, which suffer from rapid degradation after several cycles due to inevitable accumulation of inactive Li_2CO_3 (Figure S29),[36] the cell assembled with CIP-composed electrolyte keeps cycling base on peroxodicarbonate species, with its formation/decomposition corroborated by in-situ Raman spectroscopy (Figure 4c). After extended cycling (above 143 cycles), polarization upon charging can be gradually observed,

which would be attributed to the diffusion and shuttling of soluble discharge product (Figure S30 and S31). We believe that the related irreversible shuttling and diffusion can be effectively restrained via morphology modification on both porous cathode materials and separators in the future.

Conclusions

In conclusion, in order to remedy the inherent defect of conventional Li-O_2/CO_2 battery and revolutionarily change the energy storage carrier from typical carbonate to peroxodicarbonate, a super-concentrated electrolyte composed of DMSO-solvated contacted ion-pair (CIP) has been introduced. During cycling, the polymeric fluid network within our rationally-introduced electrolyte system effectively stabilizes the peroxodicarbonate by interdicting its further reduction into Li_2CO_3, which successfully lead to obviously decreasing of charge potential (from 4.2 to 3.5 V) and remarkable boost the energy efficiency. For the first time, the Li_2CO_3-free Li-O_2/CO_2 battery cycles via pure peroxodicarbonate formation has been realized, and rigorously corroborated by sufficient in/ex-situ characterizations. In addition, based on the formation/decomposition of peroxodicarbonate species, rate-capability and cyclability has been well achieved in specific Li-O_2/CO_2 battery system, which delivers a relatively good stability upon cycling. In general, not being limited into Li-O_2/CO_2 battery, the unique features of super-concentrated electrolyte strategy would provide an enlightening insight to the construction of various advanced electrochemical energy storage application. Moreover, we anticipate that the stabilization of peroxodicarbonate species would accelerate the step of evolution from Li-O_2 to practical Li-ambient air battery, as well as to other possible utilization into field of CO_2 capturing.

Acknowledgements

This work was partially supported by SPRING-ALCA from the Japan Science and Technology Agency (JST). The financial support from the National Basic Research Program of China (2014CB932300) and NSF of China (21373111 and 21633003) are acknowledged. Y. Q. acknowledges a scholarship from the China Scholarship Council (CSC).

Notes and references

1 P. G. Bruce, S. A. Freunberger, L. J. Hardwick and J.-M. Tarascon, *Nat. Mater.*, 2012, **11**, 19-29.
2 A. C. Luntz and B. D. McCloskey, *Chem. Rev.*, 2014, **114**, 11721-11750.
3 H. K. Lim, H. D. Lim, K. Y. Park, D. H. Seo, H. Gwon, J. Hong, W. A. Goddard, H. Kim and K. Kang, *J. Am. Chem. Soc.*, 2013, **135**, 9733-9742.
4 S. S. Zhang, K. Xu and J. Read, *Journal of Power Sources*, 2011, **196**, 3906-3910.
5 J.-G. Zhang, D. Wang, W. Xu, J. Xiao and R. E. Williford, *Journal of Power Sources*, 2010, **195**, 4332-4337.
6 S. Xu, S. Lau and L. A. Archer, *Inorg. Chem. Front.*, 2015, **2**, 1070-1079.
7 T. Liu, M. Leskes, W. J. Yu, A. J. Moore, L. N. Zhou, P. M. Bayley, G. Kim and C. P. Grey, *Science*, 2015, **350**, 530-533.
8 F. J. Li, S. C. Wu, D. Li, T. Zhang, P. He, A. Yamada and H. S. Zhou, *Nat. Common.*, 2015, **6**, 8843.
9 J. L. Roberts, T. S. Calderwood and D. T. Sawyer, *J. Am. Chem. Soc.*, 1984, **106**, 4667-4670.
10 J. D. Wadhawan, P. J. Welford, E. Maisonhaute, V. Climent, N. S. Lawrence, R. G. Compton, H. B. McPeak and C. E. W. Hahn, *J. Phys. Chem. B*, 2001, **105**, 10659-10668.
11 S. R. Gowda, A. Brunet, G. M. Wallraff and B. D. McCloskey, *J. Phys. Chem. Lett.*, 2013, **4**, 276-279.
12 W. Yin, A. Grimaud, F. Lepoivre, C. Yang and J. M. Tarascon, *J. Phys. Chem. Lett.*, 2017, **8**, 214-222.
13 K. Takechi, T. Shiga and T. Asaoka, *Chem. Commun.*, 2011, **47**, 3463-3465.
14 Y. Liu, R. Wang, Y. Lyu, H. Li and L. Chen, *Energy Environ. Sci.*, 2014, **7**, 677-681.
15 C. Ling, R. Zhang, K. Takechi and F. Mizuno, *J. Phys. Chem. C*, 2014, **118**, 26591-26598.
16 B. D. McCloskey, R. Scheffler, A. Speidel, G. Girishkumar and A. C. Luntz, *J. Phys. Chem. C*, 2012, **116**, 23897-23905.
17 B. D. McCloskey, A. Speidel, R. Scheffler, D. C. Miller, V. Viswanathan, J. S. Hummelshoj, J. K. Norskov and A. C. Luntz, *J. Phys. Chem. Lett.*, 2012, **3**, 997-1001.
18 M. M. O. Thotiyl, S. A. Freunberger, Z. Q. Peng and P. G. Bruce, *J. Am. Chem. Soc.*, 2013, **135**, 494-500.
19 M. He, K. C. Lau, X. Ren, N. Xiao, W. D. McCulloch, L. A. Curtiss and Y. Wu, *Angew. Chem. Int. Ed.*, 2016, **55**, 1-6.
20 B. Liu, W. Xu, P. Yan, S. T. Kim, M. H. Engelhard, X. Sun, D. Mei, J. Cho, C.-M. Wang and J.-G. Zhang, *Adv. Energy Mater.*, 2017, doi: 10.1002/aenm.201602605.
21 R. Tatara, D. G. Kwabi, T. P. Batcho, M. Tulodziecki, K. Watanabe, H.-M. Kwon, M. L. Thomas, K. Ueno, C. V. Thompson, K. Dokko, Y. Shao-Horn and M. Watanabe, *J. Phys. Chem. C*, 2017, **121**, 9162-9172.
22 Y. Yamada, K. Furukawa, K. Sodeyama, K. Kikuchi, M. Yaegashi, Y. Tateyama and A. Yamada, *J. Am. Chem. Soc.*, 2014, **136**, 5039-5046.
23 L. Suo, Y.-S. Hu, H. Li, M. Armand and L. Chen, *Nat. Common.*, 2013, **4**, 1481.
24 L. Johnson, C. M. Li, Z. Liu, Y. H. Chen, S. A. Freunberger, P. C. Ashok, B. B. Praveen, K. Dholakia, J. M. Tarascon and P. G. Bruce, *Nat. Chem.*, 2015, **7**, 1091-1099.
25 Z. Q. Peng, S. A. Freunberger, Y. H. Chen and P. G. Bruce, *Science*, 2012, **337**, 563-566.
26 C. O. Laoire, S. Mukerjee, K. M. Abraham, E. J. Plichta and M. A. Hendrickson, *J. Phys. Chem. C*, 2010, **114**, 9178-9186.
27 Z. Q. Peng, S. A. Freunberger, L. J. Hardwick, Y. H. Chen, V. Giordani, F. Barde, P. Novak, D. Graham, J. M. Tarascon and P. G. Bruce, *Angew. Chem. Int. Ed.*, 2011, **50**, 6351-6355.

28 N. Mozhzhukhina, L. P. M. De Leo and E. J. Calvo, *J. Phys. Chem. C*, 2013, **117**, 18375-18380.
29 Y. Qiao, J. Yi, S. Wu, Y. Liu, S. Yang, P. He and H. Zhou, *Joule*, 2017, **1**, 359-370.
30 S. Yang, P. He and H. Zhou, *Energy Environ. Sci.*, 2016, **9**, 1650-1654.
31 Y. H. Chen, S. A. Freunberger, Z. Q. Peng, O. Fontaine and P. G. Bruce, *Nat. Chem.*, 2013, **5**, 489-494.
32 W.-J. Kwak, D. Hirshberg, D. Sharon, M. Afri, A. A. Frimer, H.-G. Jung, D. Aurbach and Y.-K. Sun, *Energy Environ. Sci.*, 2016, **9**, 2334-2345.
33 S. Winstein and G. Robinson, *J. Am. Chem. Soc.*, 1958, **80**, 169-181.
34 B. D. McCloskey, A. Valery, A. C. Luntz, S. R. Gowda, G. M. Wallraff, J. M. Garcia, T. Mori and L. E. Krupp, *J. Phys. Chem. Lett.*, 2013, **4**, 2989-2993.
35 Z. Liu, Y. Zhang, C. Jia, H. Wan, Z. Peng, Y. Bi, Y. Liu, Z. Peng, Q. Wang, H. Li, D. Wang and J.-G. Zhang, *Nano Energy*, 2017, **36**, 390-397.
36 Z. Zhang, Q. Zhang, Y. Chen, J. Bao, X. Zhou, Z. Xie, J. Wei and Z. Zhou, *Angew. Chem. Int. Ed.*, 2015, **54**, 6550-6553.
37